Chapter 18
Scaling Technique

Abstract Physical scaling has been successfully applied throughout the development of fire safety science in the past several decades. It is a very powerful and cost-effective tool to obtain valuable information concerning, for example, fire characteristics, smoke movement, smoke control, fire development, and fire suppression. Typical scaling techniques that have been developed are summarized in this chapter to provide a theoretical benchmark and support for further development of more advanced scaling methods. Different scaling techniques are introduced although the focus is on the Froude scaling method which is the most common one used in fire safety science. Scaling of convective heat transfer, radiative heat transfer, and heat conduction is investigated as well as scaling of water sprays, response time of sprinklers, and combustible materials.

Keywords Scaling · Heat transfer · Water spray · Combustible material · Enclosure fire · Tunnel fire

18.1 Introduction

The physical scaling has been widely used in fire safety science community. Its application permeates nearly every aspect of fire research, from free plumes to fire suppression. Despite its introduction of simplification in various applications, the scaling technique has significantly improved our understanding of fire dynamics. Heskestad [1] reviewed scaling techniques, mainly pressure modeling and Froude modeling. These are the two main techniques that have been used. Quintiere [2] also reviewed the scaling applications in fire research with a focus on ceiling jets, burning rate, flame spread, and enclosure fires. Ingason [3] carried out numerous studies on fire development in rack-storage fires, both in large scale and model scale. The in-rack conditions were found to scale very well. Perricone et al. [4] investigated the thermal response of a steel tube covered by insulating materials using scaling principles. However, the scaling laws used for the thick insulating materials may not be accurate. Cross and Xin [5] examined the scaling of wood crib fires and found good agreement between different scales. Li and Hertzberg [6] conducted a scaling study of heat conduction and heat balance in a room fire. They carried out two series of

H. Ingason et al., *Tunnel Fire Dynamics,* DOI 10.1007/978-1-4939-2199-7_18

room fire tests in three different scales where the aim was to investigate the scaling of temperatures inside the walls. A good agreement between different scales was found.

Scaling of water-based fire suppression systems has also been conducted in open and enclosure fires. Heskestad [7, 8] carried out a series of gas and pool fire suppression tests to investigate the credibility of scaling the interaction of water sprays and flames, and obtained a simple correlation for extinguishment of gas and pool fires using water sprays. Quintiere et al.'s work [9] showed that the scaling of pool and gas fires worked well, although the results in rack-storage fires between model and full scale did not show a good correlation. Yu et al. [10–12] tested and investigated the scaling of suppression of gas fires and pool fires using water mist systems and obtained good agreement between model scale and full scale. In short, despite much work on scaling of water-based fire suppression systems, the phenomena in reality are not well understood.

In the field of tunnel fire safety, scaling techniques are widely used. The main reason promoting their applications is the high cost of full-scale tunnel tests. Note that even in model scales, the ratio of tunnel length to tunnel height should be great enough to scale a realistic tunnel fire. Fortunately the introduction of longitudinal flows allows us to slightly reduce the scaling ratio, compared to an enclosure fire. A large number of model scale tunnel fire tests have been carried out in the past two decades. Bettis et al. [13] carried out nine fire tests using scale models of vehicles in a model tunnel to mimic part of a train used to transport HGVs through the Channel tunnel. Oka and Atkinson [14] carried out a study of critical velocity in a model tunnel. Further, Wu and Bakar [15] carried out tests to investigate the influence of tunnel geometry on the critical velocity. Ingason and Li investigated the key parameters for large fires in model scale tunnels with longitudinal ventilation [16] and with point extraction ventilation [17]. Ingason [18] also carried out a series of 1:10 scale model railcar tunnel fire tests to investigate the effect of openings on the fire sizes. Vauquelin et al. [19] carried out a series of model scale experiments with a helium/nitrogen gas mixture in an isothermal test-rig to investigate the extraction capability and efficiency of a two-point extraction system. Li and Ingason [17] pointed out that the cold gas method used by Vauquelin et al. [19] results in experimental inaccuracy, and therefore is not recommended to use in tunnel fire tests. Li et al. [20–24] carried out several series of model scale tunnel fire tests to investigate the critical velocity [20], back-layering length [20], maximum ceiling gas temperature [21, 22], smoke control in cross-passages [23], and smoke control in rescue stations in long-railway tunnels [24]. Lönnermark et al. [25] carried out a 1:3 model-scale metro car fire tests in preparation for the full-scale fire tests in the Brunsberg tunnel [26].

Model-scale tunnel fire tests with water-based fire suppression have also been carried out. Ingason [27] tested the water spray system in tunnel fires using hollow cone nozzles and wood crib fires. Deluge system and water curtain system were tested. Li and Ingason [28, 29] investigated the automatic water spray system in tunnel fires using full cone nozzles and wood crib fires. Response times for individual sprinklers were modeled using a scaling theory.

18.2 Methods of Obtaining Scaling Correlations

There are two main approaches for obtaining scaling correlations: the controlling equation method, and the dimensional analysis. The controlling equation method introduces normalizing parameters and obtains nondimensional equations. The dimensionless groups are typically the coefficients of the differential terms. For the dimensional analysis method, all the key parameters relevant to the phenomenon need to be determined manually, and then the dimension of every identified parameter is changed to a combination of the basic physical dimensions. The dimensionless groups can thus be obtained by checking the dimensions of the identified physical parameters. The method could, for example, be a π theorem. There are some other methods that could be used. For example, some dimensionless groups could be directly obtained from some basic equations; but, this method is still the differential method.

In any case, the controlling equation method is the fundamental and typically best method, which will be used in the following. Nonetheless, good understanding of the phenomena is required to determine the key parameters that must be preserved.

18.3 Classification of Scaling Techniques

The scaling techniques applied in fire safety can be classified into three types: Froude scaling, pressure scaling, and analogy scaling.

18.3.1 Froude Scaling

Froude scaling indicates that the main preserved dimensionless group in the fire tests is the Froude number which characterizes the ratio of inertial force and buoyancy force. Note that all the smoke flows are driven by the buoyancy. This is the main reason why Froude scaling works by simply preserving the Froude number.

According to Froude scaling, the tests can be carried out in ambient environment. The Reynolds number is not preserved but the fluid mode should be kept the same to preserve the similarity in the fluid field. Further, many related dimensionless groups that are implicitly preserved, however, have been proved to be reasonably scaled.

18.3.2 Pressure Scaling

Pressure scaling can preserve both the Froude number and the Reynold number by adjusting the environmental pressure in the test bed. This also indicates the preservation of the Grashof number. Therefore, both the buoyancy force and the fluid

field can be scaled well. However, in reality the pressure scaling is very difficult to use since the pressure scales as 3/2 power of the length scale. This implies that the pressure needs to be adjusted to very high levels in model scale, for example, 32 atmospheres for a scaling ratio of 1:10, and 89 for a scaling ratio of 1:20. This limits its use in fire modeling. Further, the benefit of pressure scaling may be quite limited since in most cases the Reynold number is much less important compared to the Froude number.

18.3.3 Analog Scaling (Cold Gas, Saltwater)

The analog scaling method uses two fluids of different densities to model smoke movement in a fire scenario. These two fluids could be air and helium, or water and saturated salt water, and so on. This method simulates a fire using the density difference, rather than the temperature difference. To some extent, it is possible to obtain the required density using different mixing ratios. The analog scaling is in fact also a type of Froude scaling, although it is significantly different from traditional Froude scaling and is, therefore, classified as an independent method. The Froude number is also the main preserved dimensionless group. Further, turbulent flow conditions can be obtained much more easily due to the small viscosity for water.

However, this method has some defects. First, when using analog scaling, the fluid density must be determined based on a reference gas temperature in a specific fire, despite the fact that it is known that the gas temperature changes significantly with position in many fire scenarios. In other words, a realistic fire has no so-called generic or characteristic gas temperature or gas density. Despite this, the state-of-the-art is to use the estimated characteristic temperature in a given scenario and then to calculate the mass flow rate from the fire source based on conservation of the convective heat release rate (HRR). This method is only useful in a typical enclosure fire where the gas temperature can be estimated accurately. Second, the heat loss to the surroundings is ignored except in the vicinity of the fire source, that is, the heat loss is considered by using the convective HRR to build up the energy equation. Generally speaking, the energy dissipates only by mixing with the ambient fluid. However, it should be kept in mind that in a tunnel fire, the heat loss to the walls dominates the heat transfer process or the change of gas temperature along the tunnel. This suggests that the analog scaling method is not suitable for research into the temperature distribution along the tunnel. Third, the analog scaling method generally can only simulate small fires. The saturated salt water is around 1200 kg/m^3 under ambient conditions. Therefore, the maximum variance in density is around 20%. However, a gas temperature of 600 °C corresponds to a variance of 67% in density. That is to say, saltwater under ambient conditions can only simulate a fire with gas temperature of around 94 °C. Finally, extra gases or liquids with a certain momentum may be introduced into the fluid domain which could result in a large error.

18.4 General Froude Scaling

In this application, the controlling equation method is used to obtain the dimensionless groups. At first, we focus on scaling of the fluid field, and detailed scaling of heat transfer will be discussed in the following sections. For simplification, we only analyze the one-dimensional conservation equations of mass, momentum, and energy which can be written as follows:

Mass:

$$\frac{\partial \rho}{\partial t} + \frac{\partial (\rho u)}{\partial x} = \dot{m}''' \tag{18.1}$$

or in terms of individuals species (mass fraction Y):

$$\frac{\partial \rho Y_i}{\partial t} + \frac{\partial (\rho u Y_i)}{\partial x} = \frac{\partial}{\partial x}(\rho D_i \frac{\partial Y_i}{\partial x}) + \dot{m}_i''' \tag{18.2}$$

Momentum:

$$\frac{\partial (\rho u)}{\partial t} + \frac{\partial (\rho u u)}{\partial x} = \frac{\partial}{\partial x}(\frac{4}{3}\mu \frac{\partial u}{\partial x}) - \frac{\partial p}{\partial x} + (\rho_o - \rho) g_x \tag{18.3}$$

Energy:

$$\left[\frac{\partial (\rho c_p T)}{\partial t} + \frac{\partial (\rho u c_p T)}{\partial x} = \frac{\partial}{\partial x}(k \frac{\partial T}{\partial x}) + \dot{Q}''' - \dot{Q}'''_{loss} + \frac{4}{3}\mu (\frac{\partial u}{\partial x})^2 + \frac{\partial p}{\partial t} + u \frac{\partial p}{\partial x} \right] \tag{18.4}$$

State equation of gas:

$$p = \frac{\overline{R}}{M} \rho T \tag{18.5}$$

where ρ is the density (kg/m^3), t is the time (s), x is the axis (m), u are the velocity at x direction (m/s), D is the mass diffusivity (m^2/s), m is the mass (kg), Y is the species mass fraction (%), μ is the dynamic viscosity (kg/(m s)), p is the pressure (Pa), g is the gravitational acceleration (m/s^2), T is the gas temperature in Kelvin (K), k is the heat conductivity (kW/mK), c_p is the heat of capacity (specific heat at constant pressure, kJ/(kg K)), $\overline{R}$ is the universal gas constant (8.314 J/(mol K)), M is the molecular weight (kJ/kmol), and Q is the heat (kJ). Subscripts i is the ith species and *loss* indicates heat loss. Superscripts (·) indicates per unit time and ($'''$) per unit volume. Note that the pressure in the equations is the absolute pressure.

The characteristic length l (m), velocity u_o (m/s), time t_o (s), pressure p_r (Pa), ambient temperature T_o (K), and ambient density ρ_o (kg/m^3) are introduced as reference values to normalize the above equations giving:

Mass:

$$\pi_1 \frac{\partial \hat{\rho}}{\partial \hat{t}} + \frac{\partial(\hat{\rho}\hat{u})}{\partial \hat{x}} = \pi_2 \tag{18.6}$$

or in terms of individuals species (mass fraction Y_i):

$$\pi_1 \frac{\partial \hat{\rho} Y_i}{\partial \hat{t}} + \frac{\partial \hat{\rho}\hat{u} Y_i}{\partial \hat{x}} = \pi_3 \frac{\partial}{\partial \hat{x}}(\hat{\rho}\frac{\partial Y_i}{\partial \hat{x}}) + \pi_4 \tag{18.7}$$

Momentum:

$$\pi_1 \frac{\partial \hat{\rho}\hat{u}}{\partial \hat{t}} + \frac{\partial \hat{\rho}\hat{u}\hat{u}}{\partial \hat{x}} = \frac{4}{3}\pi_5 \frac{\partial^2 \hat{u}}{\partial \hat{x}^2} - \pi_6 \frac{\partial \hat{p}}{\partial \hat{x}} + \pi_7(1-\hat{\rho}) \tag{18.8}$$

Energy:

$$\pi_1 \frac{\partial \hat{\rho}\hat{T}}{\partial \hat{t}} + \frac{\partial \hat{\rho}\hat{u}\hat{T}}{\partial \hat{x}} = \pi_8 \frac{\partial^2 \hat{T}}{\partial \hat{x}^2} + \pi_9 - \pi_{10} + \pi_{11}\frac{4}{3}(\frac{\partial \hat{u}}{\partial \hat{x}})^2 + \pi_1\pi_{12}\frac{\partial \hat{p}}{\partial \hat{t}} + \pi_{12}\frac{\partial \hat{p}}{\partial \hat{x}} \tag{18.9}$$

In the above equations, the dimensionless variables, that is, the parameter divided by the corresponding reference value, are denoted by (^), for example, $\hat{\rho} = \rho / \rho_o$. Note that the convection terms are the primary terms that need to be preserved. Therefore, these are used as the basis while obtaining the dimensionless groups. Further, note that the pressure rise in a normal fire scenario is very small compared to the ambient pressure, and thus the state equation is always applicable and it needs no special attention.

The dimensionless groups obtained are listed below.

Mass:

$$\pi_1 = \frac{l}{u_o t_o}, \quad \pi_2 = \frac{\dot{m}''' l}{\rho_o u_o}, \quad \pi_3 = \frac{D_i}{u_o l}, \quad \pi_4 = \frac{\dot{m}_i''' l}{\rho_o u_o} \tag{18.10}$$

Momentum:

$$\pi_5 = \frac{\mu}{\rho_o u_o l}, \quad \pi_6 = \frac{p_r}{\rho_o {u_o}^2}, \quad \pi_7 = \frac{gl}{{u_o}^2} \tag{18.11}$$

Energy:

$$\begin{aligned} &\pi_8 = \frac{k}{\rho_o u_o c_p l}, \quad \pi_9 = \frac{\dot{Q}''' l}{\rho_o u_o c_p T_o}, \quad \pi_{10} = \frac{\dot{Q}'''_{loss} l}{\rho_o u_o c_p T_o}, \\ &\pi_{11} = \frac{\mu}{\rho_o c_p T_o l}, \quad \pi_{12} = \frac{p_r}{\rho_o c_p T_o} \end{aligned} \tag{18.12}$$

Note that:

$$\pi_7 = \frac{gl}{u_o^{\,2}} = \frac{1}{\mathrm{Fr}}, \qquad \frac{\pi_5}{\pi_3} = \mathrm{Sc}, \qquad \frac{\pi_5}{\pi_8} = \mathrm{Pr}, \qquad \pi_5 = \frac{1}{\mathrm{Re}} \tag{18.13}$$

where Re is the Reynolds number, Fr is the Froude number, Sc is the Schmidt number, and Pr is the Prandtl number. Now we check which terms could be preserved in the scaling. First we know for buoyancy driven flows, the Froude number, that is, π_7, has to be preserved. To preserve the transient characteristics of the key parameters, the time derivative term has to be preserved, that is, π_1. Therefore, we have:

$$u \propto t \propto l^{1/2} \tag{18.14}$$

This indicates that the velocity and time scales as 1/2 power of the length scale. In other words, if the geometrical scale ratio is L_M/L_F (model scale M and full scale F), the velocity and the time scale as $u_M/u_F = t_M/t_F = (L_M/L_F)^{1/2}$.

Further, the source terms, including mass source (π_2 and π_4) and heat source terms (π_9 and π_{10}), need to be preserved, especially the heat source terms. To preserve mass source terms, we have:

$$\dot{m} \propto \dot{m}_i \propto l^{5/2} \tag{18.15}$$

To preserve heat source terms, we have:

$$\dot{Q} \propto \dot{Q}_{loss} \propto l^{5/2} \tag{18.16}$$

By preserving the above terms, it can be concluded that the temperature should approximately be the same between different scales. Further, note that if different fuels are used, the mass and energy cannot be simultaneously scaled. The heat terms should always have higher priority in such cases.

Further we check each term in the three controlling equations. From the mass equation it can be known that the mass should be scaled very well. Even when the fuel mass is not scaled well, good agreement can still be found in different scales since the fuel mass is normally negligible in the smoke flow. For the species equation, the concentrations should be scaled well if the mass source is scaled correctly.

Note that by default the dynamic pressure is proportional to the second power of the velocity. In addition, from the momentum equation, it can be seen that the buoyancy forces have been scaled. Given that the viscous term is negligible compared to the buoyancy in most cases, the pressure term should be scaled as:

$$p_r \propto l \tag{18.17}$$

This indicates that the pressure rise is proportional to the length scale.

From the energy equation, it can be known that the heat source is scaled but not the diffusion terms and the pressure terms. However, this is much less important.

Further, note that the heat loss term could not be scaled very well, but the influence should be limited, especially close to the fire source since the majority of the heat is carried away by the convective flows. Therefore, the energy should be scaled well.

In short, all the key terms are scaled, including the time derivative terms. Therefore, the basic theory of Froude scaling works well.

By checking the theory for turbulent flows, we can have an interesting finding. Note that the viscous stress cannot be preserved for laminar flows as discussed above. However, for turbulence flows, we can easily find that all turbulent diffusion terms can be scaled well in both Reynolds-averaged Navier–Stokes (RANS) models and Large Eddy simulations (LES) models. This suggests that Froude scaling works better in turbulent flows. Therefore, in carrying out model scale tests we should try to have turbulent flows in mode scales.

Note that in enclosure fires or tunnel fires, heat transfer to the surrounding structures needs to be carefully considered which will be discussed in the following section.

18.5 Scaling of Heat Fluxes

Scaling of heat conduction, convective heat transfer, and radiative heat transfer are presented in the following. Finally, the scaling of heat balance in an enclosure is presented.

18.5.1 Scaling of Convective Heat Transfer

In an enclosure fire or a tunnel fire, the key pattern of the convective heat transfer is the forced heat transfer due to the movement of the hot gases in the upper layer and also the forced heat transfer in the lower layer due to the movement of fresh air through the openings. The main mechanism should, therefore, be forced convective heat transfer. The convective heat transfer to the walls, $\dot{Q}_{loss,c}$, can be expressed as:

$$\dot{Q}_{loss,c} = h_c A_w (T_g - T_w) \tag{18.18}$$

where h_c is the convective heat transfer coefficient (kW/(m^2 K)), A_w is the contact wall surface area (m^2), T_g is the gas temperature (K), and T_w is the wall temperature (K). This suggests that the convective heat flux should scale as 1/2 power of the length scale. In the following, we examine the actual scaling correlations for different flow modes on smooth and rough surfaces to check whether they follow this law.

For turbulent flows on smooth wall surfaces, the convective heat transfer coefficient h_c could be correlated with the Nusselt Number and the Prandtl number:

$$\mathrm{Nu} = \frac{h_c l}{k} = 0.037\,\mathrm{Re}^{4/5}\,\mathrm{Pr}^{1/3} \tag{18.19}$$

The above equations indicate that:

$$\dot{q}_c'' \propto h_c \propto l^{1/5} \tag{18.20}$$

For laminar flows on smooth surfaces, the convective heat transfer coefficient h_c can also be correlated with the Nusselt Number and the Prandtl number, which can be expressed as:

$$\mathrm{Nu} = \frac{h_c l}{k} = 0.66\,\mathrm{Re}^{1/2}\,\mathrm{Pr}^{1/3} \tag{18.21}$$

This means that:

$$\dot{q}_c'' \propto h_c \propto l^{-1/4} \tag{18.22}$$

For a heated wall at the lower layer in an enclosure fire, the convective heat transfer could be natural convection, and the Nusselt number could be expressed as:

$$\mathrm{Nu}_L = 0.678\,\mathrm{Ra}_L^{1/4}\left(\frac{\mathrm{Pr}}{\mathrm{Pr}+0.952}\right) \tag{18.23}$$

where the Rayleigh number, Ra_L, is defined as:

$$\mathrm{Ra}_L = \frac{g\beta\Delta T L^3}{\nu^2}\mathrm{Pr} \tag{18.24}$$

In the above equation, ν is the kinematic viscosity (m^2/s), β is the expansion coefficient (equivalent to $1/T$ for ideal gas in an isobaric process). From the above equation we also obtain the scaling coefficient of $-1/4$.

Note that some tunnel walls could be very rough, for example, rock tunnel walls. The expressions for the Nusselt number needs to be revised to account for the effect of wall roughness. Recall the Reynold-Colburn analogy:

$$St = \frac{h_c}{\rho c_p u} \approx \frac{1}{2} C_f \tag{18.25}$$

For turbulent flows on rough surfaces, the skin friction coefficient, C_f, mainly depends on the relative roughness, and approaches a constant at high Reynolds numbers for each relative roughness, ε/D. Therefore, if the relative roughness is kept as the same value in both scales and the flow mode is turbulent, the convective heat flux scales as:

$$h_c \propto u \propto l^{1/2} \tag{18.26}$$

This suggests that the convective heat flux can scale very well if the flow is turbulent and the relative roughness is kept as the same value in model scale. In reality, the requirement for the conservation of the relative roughness could be eased due to the fact that the friction coefficient is not so sensitive to the wall roughness. Generally for turbulent flows, the relative roughness for tunnel walls range from 0.1 to 1 %, corresponding to a skin friction coefficient, C_f, ranging from 0.08 to 0.16.

Based on the above analysis, it is known that the convective heat transfer can be scaled very well for turbulent flows in model tunnels with the same relative roughness. The convective heat transfer for laminar flows in model scales could be slightly overestimated.

18.5.2 Scaling of Radiative Heat Transfer

The scaling of radiative heat transfer on the wall surface, $\dot{q}''_{w,r}$ (kW/m^2), can be expressed as:

$$\dot{q}''_{w,r} = \varepsilon_w \int_{2\pi} I d\Omega - \varepsilon_w \sigma T_w^4 \tag{18.27}$$

where ε_w is emissivity of the wall surface, I is intensity of incident radiation (kW/(m^2 steradium)), Ω is solid angle, and σ is the Stefan-Boltzmann constant (5.67×10^{-11} kW/(m^2 K^4)).

Using the controlling equation method to normalize the above controlling equation, we can easily obtain the following scaling correlations:

$$\pi_{13} = \frac{\dot{q}''_{w,r}}{\varepsilon_w \sigma T_o^4}, \qquad \pi_{14} = \frac{I_o}{\sigma T_o^4} \tag{18.28}$$

Note that the dimensionless group π_{14} indicates the definition of radiation intensity. The other dimensionless group suggests the scaling of wall emissivity:

$$\varepsilon_w \propto l^{1/2} \tag{18.29}$$

Generally the emissivity of the walls is not scaled. This suggests that the radiation at the wall is normally overestimated in model scales, which tends to reduce the vertical temperature difference.

Now let us analyze the scaling of radiative heat transfer in a fluid element. The radiation transport equation (RTE) is:

$$\frac{dI}{dx} = -\kappa\left(I - \frac{\sigma T^4}{\pi}\right) \tag{18.30}$$

where κ is the absorption coefficient (1/m).

For a fluid element, the term in the energy equation related to heat loss by radiation can be written as:

$$\dot{Q}'''_{loss,r} = 4\kappa\sigma T^4 - \kappa\int_{4\pi} I d\Omega \tag{18.31}$$

where Ω is the solid angle (steradian). Using the controlling equation method we can easily obtain the following scaling correlations:

$$\pi_{15} = \kappa l, \qquad \pi_{16} = \frac{\dot{Q}'''_{loss,r}}{\kappa\sigma T_o^4} \tag{18.32}$$

These two dimensionless groups indicate:

$$\kappa \propto l^{-1}, \qquad \kappa \propto l^{-1/2} \tag{18.33}$$

In an enclosure fire or a tunnel fire, the soot normally dominates the absorption coefficient, and thus the absorption coefficient in different scales should be essentially the same, if the same fuels are used. Therefore the local absorption coefficient cannot be scaled well, and both the local absorbed heat and the outgoing radiation may be underestimated. Thus the overall effect is difficult to estimate.

However, note that this conclusion is drawn from the analysis of a fluid element. In fact, in enclosure fires, scaling of the global radiative heat transfer is more meaningful and of more practical use. From the global point of view, the radiative heat transfer from the flame and hot gases to the walls can be expressed in a similar way as the convective heat transfer, that is, as:

$$\dot{Q}_{loss,r} = h_r A_w (T_g - T_w) \tag{18.34}$$

For simplicity, the radiative heat transfer coefficient for the wall surfaces could be written as follows:

$$h_r = \varepsilon\sigma(T_g^2 + T_w^2)(T_g + T_w) \tag{18.35}$$

where the emissivity is:

$$\varepsilon = 1 - e^{-\kappa_m L_m}$$

In the above equations, h_r is the equivalent radiative heat transfer coefficient (kW/(m^2 K)), κ_m and L_m are the mean absorption coefficient (1/m) and mean beam length of the flame and smoke flow (m), respectively.

It is clear that the emissivity of the gas in model scale normally becomes smaller than in full scale, however, the emissivity strongly depends on the length scale and thus in reality is very difficult to estimate. Here we make a simple analysis of the optically thick and optically thin cases. In the optically thick case, the emissivity is close to unit. Therefore scaling of the global radiative heat flux is:

$$\dot{q}_r'' \propto l^0 \tag{18.36}$$

In the optically thin case, scaling of radiative heat flux could be:

$$\dot{q}_r'' \propto \kappa_m L_m \propto l^1 \tag{18.37}$$

Note that the radiative heat flux is the inverse of the radiative resistance R_r. At the beginning of an enclosure fire, the scenario is optically thin. However, after a period of time, the scenario could become optically thick. Therefore, the radiative heat flux could be scaled as l^a $(0<a<1)$. Note that the heat flux should scale as $l^{1/2}$. It could be expected that in the model scale, the radiative heat flux may be underestimated at the beginning of the fire and overestimated a short time after ignition. We can also try to ascertain the coefficient a in the optically thick case.

The absorption coefficient is mainly dependent on the soot yields and volumetric flow rate of the smoke. In other words, it depends on the fuel type, ventilation conditions, and specific geometry of the room and the burner. In model scales, if the fuels are the same as in full scale, it can be expected that the absorption coefficient is also the same as in full scale, given that the ventilation conditions and specific geometry are well scaled. Therefore, the scaling of radiative heat flux is mainly related to the mean beam length. In engineering applications, the global radiative heat flux could be calculated using a mean beam length, L_m, which could be estimated by:

$$L_m = 3.6\frac{V_b}{A_b} \tag{18.38}$$

where V_b is the volume of the hot gases (m^3) and A_b is its bounding area (m^2). The mean beam length in an enclosure fire is mainly related to the smoke depth. Therefore, it is a variable for different fire sizes. For large flames and sooty smoke, the emissivity always approaches one and the mean beam length has no influence on the radiation. However, for small fires, both the absorption coefficient and the smoke depth are small values, and thus the mean beam length could play an important role in the total emissivity.

We may choose different fuels in model scales to explicitly scale the radiative heat flux in enclosure fires. However, it should be kept in mind that the absorption coefficient is not only related to the fuel type and HRR, but also the length scale, the entrainment of the smoke flows, and the combustion conditions, for example, an under-ventilated fire produces much more soot. In realistic fires, the absorption coefficient could be a time-dependent variable during a fire. In any case, the scaling of radiation is difficult based on the above analysis. In reality, the fire scales the radiation itself as there is limited heat available to be lost by radiation. Therefore in a real fire, the temperature will decrease if the emissivity is too high in model scales. The radiation fraction in the total HRR in open fires and enclosure fires has been observed to be around 20–40 %. This mainly results from the self-adjustment of the heat radiation. Although the gas temperature could decrease in model scales,

the difference in gas temperature between different scales could still be insignificant since heat radiation is proportional to the fourth power of gas temperature. In short, the scaling of radiative heat transfer is still expected to be acceptable in model scales, as proved by Li and Hertzberg [6].

18.5.3 Scaling of Heat Conduction

18.5.3.1 Thermally Thick Materials

In most cases, heat conduction normal to a wall surface dominates heat conduction into the wall. Therefore, only the one-dimensional heat conduction equation for the material temperature is discussed here.

The wall materials can be classified into two categories: thermally thick materials and thermally thin materials. For a thermally thick material, there is always a temperature gradient inside the material, even after thermal penetration. This state is important when considering temperatures created by fires. For a thermally thin material, the temperatures inside the material are homogeneous. In fact, thermally thin materials are only special case of thermally thick materials. There is no clear distinction between these two types of "materials," but the definition will depend on the specific case that is investigated. Generally, metal objects and very thin materials and can be considered as thermally thin materials, and others are thermally thick materials.

For thermally thick materials, the controlling equation for heat conduction can be written as:

$$\rho_s c_s \frac{\partial T_s}{\partial t} = k_s \frac{\partial^2 T_s}{\partial z^2} \tag{18.39}$$

and the boundary condition at $z=0$ and $z=\delta_s$, can be expressed as:

$$k_s \frac{\partial T_s}{\partial z} = \dot{q}_c'' + \dot{q}_r'' \tag{18.40}$$

In the above equations, z is the depth below surface (m). Subscript s indicates solid, c and r are convective and radiative heat transfer, respectively.

In the following analysis, it is assumed that the convective and radiative heat fluxes at the surface scale as 1/2 power of the length scale.

By introducing the following normalizing parameters: reference time, t_o, reference temperature, T_o, and reference material thickness, δ_s, the above equations can be normalized:

$$\frac{\partial \hat{T}_s}{\partial \hat{t}} = \frac{k_s t_o}{\rho_s c_s \delta_s^2} \frac{\partial^2 \hat{T}_s}{\partial \hat{z}^2} \tag{18.41}$$

and

$$\frac{\partial \hat{T}_s}{\partial \hat{z}} = \frac{(\dot{q}_c'' + \dot{q}_r'')\delta_s}{k_s T_o} \tag{18.42}$$

yielding the dimensionless groups:

$$\pi_{17} = \frac{k_s t_o}{\rho_s c_s \delta_s^2} \tag{18.43}$$

and

$$\pi_{18} = \frac{(\dot{q}_c'' + \dot{q}_r'')\delta_s}{k_s T_o} \tag{18.44}$$

Note that as $\dot{q}_c'' \propto l^{1/2}$ and $\dot{q}_r'' \propto l^{1/2}$, the above two equations indicate that:

$$\frac{\rho_s c_s \delta_s^2}{k_s} \propto l^{1/2} \tag{18.45}$$

and

$$\frac{\delta_s}{k_s} \propto l^{-1/2} \tag{18.46}$$

Introducing (18.44) into (18.43) suggests:

$$k_s \rho_s c_s \propto l^{3/2} (\text{thermal inertia}) \tag{18.47}$$

and

$$\frac{k_s}{\delta_s} \propto l^{1/2} (\text{thickness}) \tag{18.48}$$

The wall materials and the noncombustible surface materials should be chosen according to the above two equations. Note that based on the scaling, the wall temperature at depth δ in the full scale generally corresponds to that at a different position in the model scale.

In the following, we simply check the scaling of heat conduction. At the beginning of an enclosure fire, that is, when the heat has not yet penetrated the walls, the conductive heat flux through wall surfaces can be written as:

$$\dot{q}_k'' = k_s \frac{dT_s}{dz} \propto \frac{k_s (T_w - T_o)}{\sqrt{k_s t / \rho_s c_s}} \tag{18.49}$$

This indicates that

$$\dot{q}_k'' \propto (k_s \rho_s c_s)^{1/2} l^{-1/4} \tag{18.50}$$

Note that as $k_s \rho_s c_s \propto l^{3/2}$, the above equation indicates:

$$\dot{q}_k'' \propto l^{1/2} \tag{18.51}$$

After a period when the thermal penetration occurs, the conductive heat flux through wall surfaces can be expressed as:

$$\dot{q}_k'' = \frac{k_s}{\delta_s}(T_w - T_{wb}) \tag{18.52}$$

Note that as $k_s / \delta_s \propto l^{3/2}$, the above equation also indicates the scaling law for the conduction heat flux.

Therefore, it is clear that the heat conduction in thermally thick materials can be scaled well if the proposed two dimensionless groups are preserved in model scale and the wall surface temperature scales well.

18.5.3.2 Thermally Thin Materials

For thermally thin materials, for example, thin wall materials or metal objects, the properties inside the materials can be assumed to be homogeneous, and the controlling equation can be simply expressed as:

$$\rho_s V_s c_s \frac{\partial T_s}{\partial t} = \dot{q}_{net}'' A_s \tag{18.53}$$

where V indicates volume (m^3) and A_s is surface area (m^2). The characteristic parameters are introduced to normalize the above equation to yield:

$$\frac{\partial \hat{T}_s}{\partial \hat{t}} = \frac{\dot{q}_{net}'' A_s t_o}{\rho_s V_s c_s T_o} \tag{18.54}$$

In this case we also assume that the convective and radiative heat fluxes are scaled well, that is, $\dot{q}_{net}'' \propto l^{1/2}$. Thus the above equation indicates the following relationship:

$$\rho_s V_s c_s \propto l^3 \tag{18.55}$$

This suggests that in order to scale the heat conduction in thermally thin materials, the same materials can be used, if the materials are geometrically scaled. In reality, scaling of the thermally thick materials also fulfills Eq. (18.55), assuming the temperatures inside the material are homogeneous or the conductivity is infinite.

Thus, as discussed previously, a thermally thin material is only a special case of a thermally thick material.

In summary, to scale the heat conduction inside thermally thick materials, Eqs. (18.45) and (18.46) need to be preserved while choosing the materials and the wall thicknesses. For thermally thin materials, the same materials can be used if the materials are geometrically scaled.

18.5.4 Scaling of Heat Balance in an Enclosure

Note that tunnels can be regarded as a special type of enclosures. The total heat released in an enclosure can be balanced by the heat loss by smoke flow exiting through openings, that is, doors and windows, $\dot{Q}_c$ (kW), and the heat loss by conduction into the walls, $\dot{Q}_k$ (kW), and the radiation through the openings, $\dot{Q}_r$ (kW), which can be expressed as follows:

$$\dot{Q} = \dot{Q}_c + \dot{Q}_k + \dot{Q}_r \tag{18.56}$$

18.5.4.1 Heat Loss by Convection Through Vents

The heat loss by convection through vents can be expressed as:

$$\dot{Q}_c = \dot{m}_g c_p (T_g - T_o) \tag{18.57}$$

where $\dot{m}_g$ is the smoke mass flow rate (kg/s) and T_g is the gas temperature (K).

In an enclosure fire, the mass flow rate of smoke flow through an opening normally can be written as:

$$\dot{m}_g \propto C_d A_o \sqrt{\Delta P} \tag{18.58}$$

where C_d is the flow coefficient (0.7 in most cases) and ΔP is the thermal pressure (Pa).

Assuming that the smoke layer can scale well and noting that the pressure difference scales as the length scale, the smoke mass flow rate through an opening should approximately scale as:

$$\dot{m}_g \propto l^{5/2} \tag{18.59}$$

For a flashover fire, which is probably ventilation controlled, the mass flow rate of the fresh air flowing into the enclosure should equal the smoke mass flow rate out of the opening, both of which can be approximately expressed as:

$$\dot{m}_a = \dot{m}_g = 0.5 A_o \sqrt{H} \propto l^{5/2} \tag{18.60}$$

where H is height of the opening (m), and $\dot{m}_a$ is the fresh air mass flow rate (kg/s).

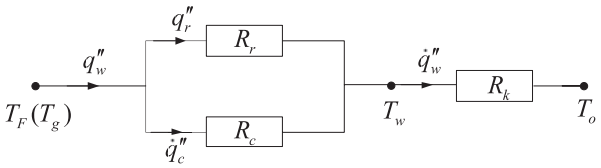

Fig. 18.1 Circuit analogy of heat loss to the walls in an enclosure fire

The heat loss by smoke flow out through the openings can be expressed as:

$$\dot{Q}_c \propto l^{5/2} \tag{18.61}$$

According to this, it is clear that the heat loss by smoke flow out through openings can scale well even for a flashover fire. In addition, it is known that a large amount of heat released in an enclosure fire is taken away by smoke flowing out of openings, which is normally called the convective HRR. The fraction of the convective HRR in the total HRR is normally in a range of 60–70 %. This is the main reason why the simplified Froude scaling can scale the fire scenario well even in model scales when the heat fluxes are implicitly scaled.

18.5.4.2 Heat Loss by Conduction into the Walls

According to the above analyses, the convective heat flux and the radiative heat flux cannot be scaled precisely as $l^{1/2}$. This definitely will affect the heat conduction inside the wall, since all the heat into the walls comes from the wall surfaces. To analyze the influence of convective and radiative heat transfer on the heat conduction in the walls, the circuit analogy of the heat loss to the walls in an enclosure fire is given, as shown in Fig. 18.1.

The total heat loss by conduction to the wall surfaces can be simply expressed as:

$$\dot{Q}_k = \dot{q}''_w A_w = h_t A_w (T_g - T_o) = A_w \frac{(T_g - T_o)}{R_t} = A_w \frac{(T_g - T_o)}{\overline{R} + R_k} \tag{18.62}$$

where the resistances are defined as:

$$R_k = \frac{1}{h_k}, \quad R_c = \frac{1}{h_c}, \quad R_r = \frac{1}{h_r}, \quad \overline{R} = \frac{R_r R_c}{R_r + R_c}$$

The conductive heat transfer coefficient, h_k (kW/m^{2}K), is defined in a similar manner as the convective heat transfer coefficient, h_c, and can easily be found for different boundary conditions. Note that $\dot{q}''_k$ is the heat flux into the wall surface, rather than heat flux deep into the wall, and the circuit analogy therefore is only a schematic description according to the relationship between the heat flux equations. Apparently, the conductive heat transfer coefficient varies with time for an unsteady state heat conduction problem.

Note that it is assumed that the radiative heat transfer is directly related to the flame or gas temperature and is proportional to the temperature difference, that is, has the same form as the convective heat transfer. However, the radiative heat transfer coefficient is not a constant except for a constant radiation temperature. The analogy is only used to clarify the interaction between different modes of heat transfer.

The above equation indicates that the all the heat resistances should be scaled as:

$$R \propto l^{-1/2} \tag{18.63}$$

Note that the lesser of R_r and R_c dominates the heat transfer to the wall surfaces. Quintiere [30] gave typical ranges for the heat transfer coefficients where $h_k \approx$ 10–30 W/(m^2 K), $h_r \approx$ 5–100 W/(m^2 K), and $h_c \approx$ 5–60 W/(m^2 K). For commonly used gypsum board, the conductive heat transfer coefficient is about 28 W/(m^2 K) in half an hour after ignition and 14 W/(m^2 K) in 1 h. We can also calculate the radiative heat transfer coefficient using Eq. (18.35). Assume that the emissivity equals 0.8 and the wall surfaces are bounded by hot gases, the radiative heat transfer coefficient is about 34 W/(m^2 K) for a gas temperature of 500 °C and 125 W/m^2·K for 1000 °C. It is clearly shown that after the gas temperature increases to about 500 °C radiation dominates the heat transfer to the wall surface. It can be expected that for a large enclosure fire, the conductive heat transfer dominates the total heat transfer from the hot gases to the surrounding walls for a long period. This means that if the heat conduction scales well, the total or overall heat transfer should also scale well in such cases. In our cases, the wall temperatures between the wall surface (T_g) and the backside (T_o) are the focus.

Note that the total heat transfer corresponds to the heat transfer from the flame and hot gases (T_g) to the penetration boundary inside the wall (T_o). However, the penetration boundary moves deeper into the wall as time goes by. Therefore, the effective thermal resistance of the wall is not constant but increases with time. For the wall temperatures at a position close to the wall surface (far away from the penetration boundary), the effective thermal resistance of the wall at the beginning of the fire cannot dominate the overall heat transfer from the hot gases to the wall, and thus the internal wall temperature does not scale very well. However, as the penetration depth increases with time, the thermal resistance becomes the dominant term in the overall heat transfer from hot gases to the internal walls. In such cases, the internal wall temperatures should scale well.

18.5.4.3 Heat Loss by Radiation Through the Vents

The heat loss by radiation through the vents could be estimated by:

$$\dot{Q}_r = \varepsilon \sigma A_o (T_g^4 - T_o^4) \tag{18.64}$$

For enclosures with small openings, the heat loss by radiation through vents can be neglected relative to other losses. However, for enclosures with large openings, the heat loss by radiation through vents should be taken into account.

The heat loss by radiation through vents scales as the radiation heat flux. Its effect on the entire heat balance mainly depends on vents area.

18.5.4.4 Global Heat Balance in an Enclosure Fire

Note that the main heat released from a fire is carried away by the smoke flows in an enclosure or a tunnel fire, which generally corresponds to 60–80 % of the total HRR. This part of the heat can be scaled well, even if the heat loss by conduction into the walls and radiation through openings are implicitly scaled. Therefore, heat flows in an enclosure fire can be scaled well. In reality, if the heat conduction is scaled as presented above, the global heat balance can be scaled better.

18.6 Scaling of Water Sprays

If water-based fire suppression systems are involved in model scale tests, additional equations need to be considered.

18.6.1 Single Droplet

At first, we analyze the equations for single water droplet.

The mass equation for a single water droplet can be expressed as [31]:

$$\frac{dm_l}{dt} = -A_l h_m \rho_l (Y_l - Y_g) \tag{18.65}$$

where

$$h_m = \frac{ShD_l}{d_l} \propto u_l^{1/2} d_l^{-1/2},$$

$$Y_l = \frac{X_l}{X_l(1 - M_a / M_l) + M_a / M_l},$$

$$X_l = \exp\left[\frac{L_v M_l}{R}\left(\frac{1}{T_b} - \frac{1}{T_l}\right)\right]$$

The momentum equation for a single water droplet is:

$$m_l \frac{d\boldsymbol{u}_l}{dt} = m_l \boldsymbol{g} - \frac{1}{8} C_d \rho_l \pi d_l^2 \left|\boldsymbol{u}_l - \boldsymbol{u}\right| (\boldsymbol{u}_l - \boldsymbol{u}) \tag{18.66}$$

where the drag coefficient, C_d, can be expressed as [32]:

$$C_d = B\,\mathrm{Re}^{-1/2} = B\left(\frac{\left|u_l - u\right| d}{v}\right)^{-1/2}$$

and

$$u_l = \frac{dx_l}{dt}$$

The energy equation for a single water droplet is:

$$m_l c_l \frac{dT_l}{dt} = h_l A_l (T_g - T_l) + h_s A_l (T_s - T_l) + \frac{dm_l}{dt}\left[c_p (T_{boil} - T_l) + L_{v,w}\right] + \dot{Q}_r \tag{18.67}$$

where

$$h_l = \frac{\mathrm{Nu}\,k}{d_l} \propto u^{1/2} d_l^{-1/2}$$

In the above equations, h_m is the mass transfer coefficient (m/s), h_l is the convective heat transfer coefficient between gas and a liquid droplet (kW/(m^2 K)), h_s is the convective heat transfer coefficient between a liquid droplet and a solid surface (kW/(m^2 K)), *Sh* is the Sherwood number, *D* is the mass diffusivity (m^2/s), *d* is the droplet diameter (m), Y_g is the vapor mass fraction, Y_l is the equilibrium vapor mass fraction, X_l is the equilibrium vapor volume fraction, $\boldsymbol{x}_l$ is the droplet trajectory (m), *B* is a constant, *c* is the heat capacity (kJ/(kg K)), C_d is the drag coefficient, A_l is exposed surface of the droplet (m^2), T_g is the gas temperature (K), u_l is the droplet velocity (m/s), *u* is the gas velocity (m/s), *k* is the conductivity of the gas (kW/(m K)), $\dot{Q}_r$ is the radiation absorbed by the droplet (kW), and $L_{v,\,w}$ is heat of vaporization of the water droplet (kJ/kg). Subscript *l* denotes the liquid, *b* the bulb, *boil* indicates the boiling state, *v* the vaporization, *s* is the solid surface, and *a* is air. Bold terms indicate vectors.

The characteristic parameters are introduced to normalize the above equations giving:

Mass:

$$\frac{d\hat{m}_l}{d\hat{t}} = -\pi_{19}(\hat{Y}_l - \hat{Y}_g) \tag{18.68}$$

Momentum:

$$\frac{d^2\hat{\boldsymbol{x}}_l}{d\hat{t}^2} = \pi_{20}\boldsymbol{g} - \pi_{21}\left|\pi_1\frac{d\hat{\boldsymbol{x}}_l}{d\hat{t}} - \hat{\boldsymbol{u}}\right|^{1/2}(\pi_1\frac{d\hat{\boldsymbol{x}}_l}{d\hat{t}} - \hat{\boldsymbol{u}}) \tag{18.69}$$

Energy:

$$\hat{m}_l\frac{d\hat{T}_l}{d\hat{t}} = \pi_{22}(\hat{T}_g - \hat{T}_l) + \pi_{23}(\hat{T}_s - \hat{T}_l) + (\pi_{24} + L_v)\frac{d\hat{m}_l}{d\hat{t}} - \hat{T}\frac{d\hat{m}_l}{d\hat{t}} + \pi_{25} \tag{18.70}$$

The dimensionless groups obtained are listed below:

$$\pi_{19} = \frac{h_m A\rho_l Y_o t_o}{m_o}, \quad \pi_{20} = \frac{t_o^2}{l}, \quad \pi_{21} = \frac{3B\rho v^{1/2}u_o^{3/2}t_o^2}{4\rho_l l d^{3/2}} \tag{18.71}$$

$$\pi_{22} = \frac{h_l A t_o}{m_{l,o}c_l}, \quad \pi_{23} = \frac{h_s A t_o}{m_{l,o}c_l}, \quad \pi_{24} = \frac{T_{boil}}{T_o}, \quad \pi_{25} = \frac{\dot{Q}_r t_o}{m_{l,o}c_l T_o} \tag{18.72}$$

Note that the dimensionless group π_1 also needs to be preserved, which also indicates that:

$$u_l \propto l^{1/2} \tag{18.73}$$

From dimensionless group π_{19} we have:

$$d_l \propto l^{1/2} \tag{18.74}$$

The correlation for the droplet diameter can also be obtained by preservation of dimensionless groups, π_{21}, π_{22}, or π_{23}. Also, note that π_{24} is always preserved. The preservation of the dimensionless group π_{25} will be discussed latter. Until now, all the dimensionless groups except π_{25} are preserved. If the radiation is insignificant, it can be expected that this scaling works very well.

18.6.2 Water Sprays

Now we consider water sprays as a whole. Note that the heat absorbed by the water spray is one of the heat loss terms for the hot gases and solid surfaces. Therefore, the water flow rate needs to be scaled as:

$$\dot{m}_l \propto l^{5/2} \tag{18.75}$$

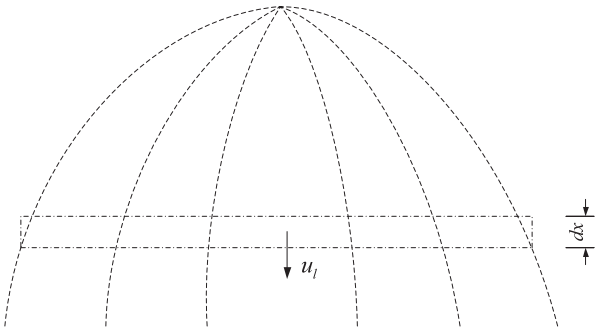

Fig. 18.2 A diagram of water sprays from one sprinkler

Further, note that initial velocity of the water spray is very important and thus needs to be scaled. Therefore, the diameter of the nozzle or sprinkler, d_n (m), needs to be geometrically scaled:

$$d_n \propto l \tag{18.76}$$

The other parameters, including the cone angle of the nozzle, spatial distribution of the water droplets, and droplet size distribution, also need to be accounted for.

Assuming that the sizes of the droplets are the same, we can estimate the total number of the droplets produced per second by the nozzle, N, as:

$$N \propto \dot{m}_l / d_l^3 \propto l \tag{18.77}$$

In the following we analyze the effect water sprays on the controlling equations for the gas flows. Figure 18.2 shows a diagram of water sprays from one sprinkler. An element with a volume of dV (m^3) and a depth of dx (m) covering the whole droplets is focused on. The average downward velocity of the droplets relative to the fluid is u (m/s), and the covered area is A (m^2). Therefore, we have:

$$dV = Adx, \quad dx = u_l dt \tag{18.78}$$

The sprays have influences on the controlling equations for the gas flows, and all the terms related to water sprays can be regarded as source terms in the controlling equations for gas flows.

Let us consider the fluid element, as shown in Fig. 18.2. It is assumed that the scaling of single water droplets works very well. Thus the source terms of the controlling equations for the fluid element due to the water sprays can be explored.

The mass source for the fluid element is:

$$\dot{m}'''_{l,tot} = \frac{N}{Au}\frac{dm_l}{dt} \propto l^{-1/2} \tag{18.79}$$

The momentum source for the fluid element is:

$$S_M = \frac{dP_l}{dx} = \frac{NdtC_d\rho_l \pi d_l^2 u_l^2}{8Adx} \propto \frac{NC_d d_l^2 u_l^2}{Au} \propto l^0 \tag{18.80}$$

The energy source for the fluid element is:

$$\dot{Q}'''_{loss} = \frac{Nm_l c_l}{Au}\frac{dT_l}{dt} \propto l^{-1/2} \tag{18.81}$$

Therefore, it can be concluded that the water sprays can be scaled well provided the single water droplet is scaled well.

18.6.3 Radiation Absorbed by Water Sprays

The absorption of radiation by water sprays is similar to the absorption of radiation by soot in the smoke flows. In a similar way, the transmittance for water sprays, τ_l, can be expressed as [7, 33]:

$$\tau_l \propto e^{-4f_v L/d_l} \tag{18.82}$$

where f_v is the volume fraction of water spray and L is the path length (m). This indicates the absorption coefficient of the water sprays scales as:

$$\kappa_l \propto f_v / d_l \propto l^{-1/2} \tag{18.83}$$

This correlates well with the obtained correlations for radiation. Heskestad [7] argues that the transmittance needs to be preserved. However, based on the above analysis, we know it should not be a constant in different scales.

As pointed out earlier, in enclosure or tunnel fires, scaling of the global radiative heat transfer is more meaningful and practical. From the global point of view, the radiative heat absorbed by the water sprays can be expressed as:

$$\dot{q}''_{r,tot} \propto \alpha_{l,tot}\sigma T^4 \tag{18.84}$$

where the absorptivity $\alpha_{l,\,tot}$:

$$\alpha_{l,tot} = 1 - e^{-\kappa_l L}$$

Note that the radiation emitted from water spray is ignored since it is much less important compared to the radiation absorbed. The above equation indicates that the absorptivity could become lower in model scales, which is reasonable according to the analysis of scaling of heat fluxes.

18.6.4 Droplet Diameter

Dombrowski et al. [34] found that the median droplet diameter is related to a Weber number, that is, the ratio of inertial forces to surface tension forces, and the correlation can be expressed as:

$$\frac{d_l}{d_n} \propto \mathrm{We}^{-1/3} \tag{18.85}$$

where the Weber number, We, is defined as:

$$\mathrm{We} = \frac{\rho_l u_n^2 d_n}{\sigma}$$

In the above equation, σ is the liquid surface tension (N/m) which can be considered as constant for a certain temperature, and u_n is the initial discharge velocity of the droplets (m/s). Therefore, the median droplet diameter produced by geometrically similar sprinkler scales as:

$$d_n \propto l^{1/3} \tag{18.86}$$

Comparing this with the previously obtained correlation shows a discrepancy for the scaling of droplet sizes. Heskestad [7] pointed out that the discrepancy may not be serious for scales varying within a moderate range.

18.6.5 Surface Cooling

According to the above analysis, water sprays are reasonably scaled before arriving at the fuel surfaces. Therefore, the mass flow rate of the water arriving at fuel surfaces, $\dot{m}_{w,s}$ (kg/s), approximately scale as:

$$\dot{m}_{w,s} \propto l^{5/2} \tag{18.87}$$

On the fuel surface, the water droplets absorb heat by evaporation to cool the fuel surface. An extinction due to surface cooling occurs when the net heat absorbed by a fuel surface decrease to a certain value, that is, the critical mass burning rate as defined by Tewarson [35] is obtained. The scaling of the heat gain and heat loss scales as:

$$\dot{m}_{w,s} L_{v,w} \approx \dot{m}_f L_{v,f} \propto l^{5/2} \tag{18.88}$$

where $\dot{m}_f$ is the fuel burning rate (kg/s) and L_v is the heat of vaporization (kJ/kg). Subscripts *w* and *f* indicate water and fuel, respectively.

This suggests that the surface cooling scales well. Note that the water sprays are also scaled well before arriving at the fuel surface. It can, therefore, be concluded that the scaling of fire suppression should be reasonably good.

18.6.6 Automatic Sprinkler

For scaling of automatic sprinklers, the response time of the bulb needs to be scaled, together with scaling of the water spray. The thermal response equation for the sprinklers can be expressed as follows [28, 29, 36–39]:

$$\frac{dT_b}{dt} = RTI^{-1}u^{1/2}(T_g - T_b) - C\cdot RTI^{-1}(T_b - T_m) - C_2\cdot RTI^{-1}X_w u \tag{18.89}$$

Where,

$$C = \frac{C'RTI}{m_b c_b}, \qquad \mathrm{RTI} = \tau u^{1/2}, \qquad \tau = \frac{m_b c_b}{h_b A_b}$$

In the above equation, RTI is the response time index ($m^{1/2}/s^{3/2}$), c is the heat of capacity (kJ/(kg K)), C is the C-Factor, C_2 is a factor accounting for the influence of upstream sprays, T_g is the gas temperature (K), T_b is the bulb temperature (K), T_m is the temperature of the sprinkler mount (close to ambient) (K), and X_w is the volume fraction of water droplets in the gas stream. Subscript b is bulb. Note that C_2 and C' are constants but C is not.

The characteristic parameters are introduced to normalize the above equation:

$$\frac{d\hat{T}_e}{d\hat{t}} = \pi_{26}(\hat{T}_g - \hat{T}_b) - \pi_{27}(\hat{T}_b - \hat{T}_m) - \pi_{28} \tag{18.90}$$

The dimensionless groups obtained are listed below:

$$\pi_{26} = \frac{u^{1/2}t_o}{\mathrm{RTI}} = \frac{h_b A_b t_o}{m_b c_b} = \frac{t_o}{\tau}, \qquad \pi_{27} = \frac{Ct_o}{\mathrm{RTI}}, \qquad \pi_{28} = \frac{C_2 u t_o X_w T_o^{-1}}{\mathrm{RTI}} \tag{18.91}$$

For sprinklers, the response time also needs to be scaled in model scales. Note that three dimensionless groups related to RTI have been obtained. To preserve π_{26}, RTI needs to be scaled as:

$$\mathrm{RTI} \propto l^{3/4} \tag{18.92}$$

To preserve π_{27}, RTI needs to be scaled as:

$$\mathrm{RTI} \propto l^{-1} \tag{18.93}$$

To preserve π_{28}, RTI needs to be scaled as:

$$\mathrm{RTI} \propto l^1 \tag{18.94}$$

Thus, comparing the three correlations shows a self-contradiction between them. Note that the ratios for π_{26} and π_{28} are close to each other, and the convective heat transfer dominates the heat balance of the element before its activation. Therefore, preservation of π_{28} is ignored. In short, RTI should be scaled as:

$$\mathrm{RTI} \propto l^{3/4} \tag{18.95}$$

It is normally impossible to obtain a very small automatic nozzle. Let us consider two methods to scale RTI. First, we can use a small cylinder with a specific material and diameter which fulfills the condition discussed later. Note that a typical sensing element can be seen as a circular cylinder. Due to the Reynolds Number being in a range of 40–4000, the convective heat transfer coefficient can be approximately expressed as:

$$h_c = \frac{kNu}{d_b} = \frac{k}{d_b} C_k \,\mathrm{Pr}^{1/3}\,\mathrm{Re}^{1/2} = C_k \,\mathrm{Pr}^{1/3}\,\frac{k}{d_b}\left(\frac{ud_b}{v}\right)^{1/2} \tag{18.96}$$

where C_k is a coefficient, d is the diameter (m), and subscript b indicates bulb. Therefore,

$$\mathrm{RTI} = \frac{m_b c_b u^{1/2}}{h_c A_b} = \frac{v^{1/2}}{4C_k \,\mathrm{Pr}^{1/3}\,k}\rho_b c_b d_b^{3/2} \tag{18.97}$$

This indicates that:

$$\rho_b c_b d_b^{3/2} \propto l^{3/4} \tag{18.98}$$

If a small cylinder can fulfill the above condition, the RTI of the element is scaled properly. The problem is that the element in model scale is generally so small that makes it impossible to produce it. The second way of scaling RTI is using a bulb with a small RTI.

18.7 Scaling of Combustible Materials

To scale the combustible materials, three basic parameters need to be preserved: geometry, HRR, and energy content. The coverage of the fuels needs to be scaled geometrically.

The HRR can be simply expressed as:

$$\dot{Q} = \dot{m}_f'' A_f \chi \Delta H_c \propto l^{5/2} \tag{18.99}$$

where $\dot{m}_f''$ is the fuel mass burning rate (kg/(m^2 s)), A_f is the fuel surface area (m^2), χ is the combustion efficiency, and ΔH_c is heat of combustion (kJ/kg).

The total energy can be estimated in the form:

$$E = m_f \chi \Delta H_c = \rho_f V_f \chi \Delta H_c \propto l^3 \tag{18.100}$$

where m_f is the fuel mass (kg) and V_f is the fuel volume (m^3).

Li et al. [40, 41] proposed a theoretical model of maximum HRRs in metro carriages which are correlated with the data from different scales of metro carriage fire tests very well. The results suggest that for scaling of the maximum HRR in a fully developed vehicle fire, the following correlation also needs to be fulfilled:

$$\frac{\Delta H_c}{L_{v,f}} \propto l^0 \tag{18.101}$$

where $L_{v,f}$ is heat of gasification of the fuel (kJ/kg).

Scaling of combustible materials is one of the most challenging tasks in physical scaling. The main problem is caused by the difficulty in choosing materials that fulfill all the requirements based on the scaling theory [40, 41]. At present, the main practical use of scaling of combustible materials is the scaling of wood crib fires.

18.8 An Example of Scaling Application in Fire Safety Engineering

Scaling applications in tunnel fires can be found in many chapters in this book, for example, gas temperature, tunnel fire ventilation, and flame length. On these specific topics, good agreement has been found between model- and large-scale tests. Therefore, they are not described further here.

The example presented here has been chosen to illustrate the scaling of internal wall temperatures in enclosure fires. Li and Hertzberg [6] proposed a method for scaling internal wall temperatures, based on which two series of enclosure fire tests were carried out in three different scales of enclosures: full scale (1:1), medium scale (1:2), and small scale (1:3.5). The method is depicted in Sect. 18.5.3. Figure 18.3 shows the comparison of the internal wall temperatures in full scale and medium scales of room fire tests with the fire source placed at the center of the room, and Fig. 18.4 shows the comparison of the internal wall temperature in full scale and small scales of the center fires. Ten percent corresponds to the location at

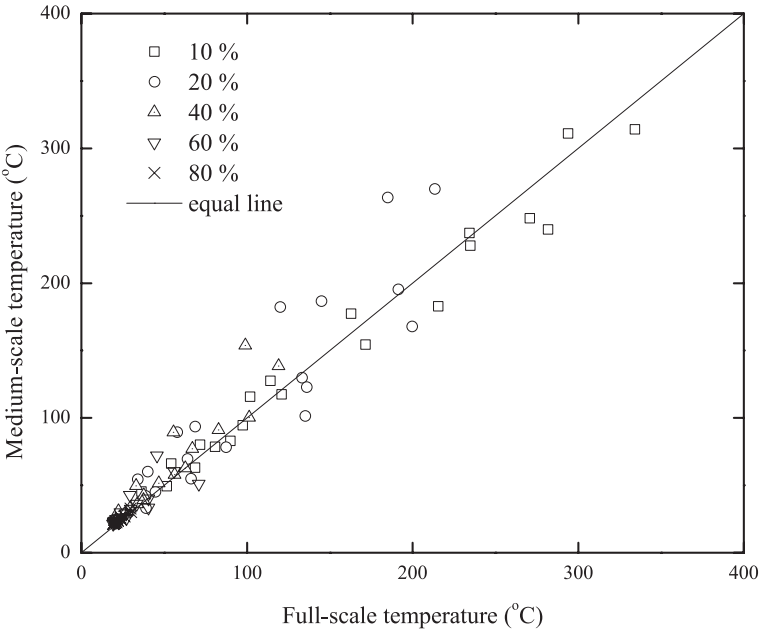

Fig. 18.3 Internal wall temperatures in full scale vs. medium scale [6]

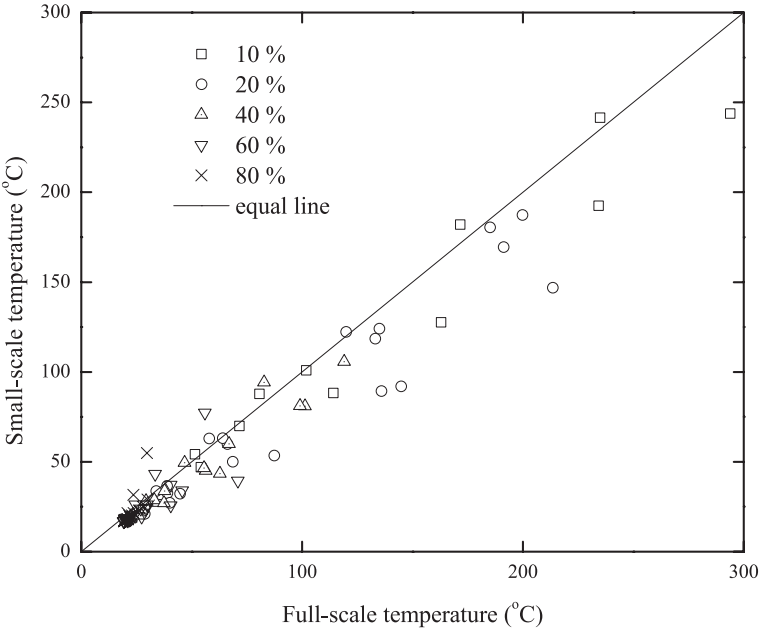

Fig. 18.4 Internal wall temperatures in full scale vs. small scale [6]

Table 18.1 A list of scaling correlations

Type of unit	Scaling
Heat release rate (HRR) (kW)	$\dot{Q}_M / \dot{Q}_F = (l_M / l_F)^{5/2}$
Velocity (m/s)	$V_M / V_F = (l_M / l_F)^{1/2}$
Time (s)	$t_M / t_F = (l_M / l_F)^{1/2}$
Energy content (kJ)	$E_M / E_F = (l_M / l_F)^3$
Mass (kg)[a]	$m_M / m_F = (l_M / l_F)^3$
Temperature (K)	$T_M / T_F = 1$
Gas concentration[a]	$Y_M / Y_F = 1$
Pressure (Pa)	$P_M / P_F = l_M / l_F$
Fuel mass burning rate (kg/(m^2 s))	$(\dot{m}''_f \Delta H_c)_M / (\dot{m}''_f \Delta H_c)_F = (l_M / l_F)^{1/2}$
Fuel density (kg/m^3)	$(\rho \Delta H_c)_M / (\rho \Delta H_c)_F = 1$
Fuel heat of pyrolysis	$(\Delta H_c / L_p)_M / (\Delta H_c / L_p)_F = 1$
Thermal inertia (kW$^2 \cdot$s$\cdot$m$^{-4} \cdot$K^{-2}))	$(k\rho c)_{s,M} / (k\rho c)_{s,F} \propto (l_M / l_F)^{3/2}$
Thickness (m)	$(k / \delta)_{s,M} / (k / \delta)_{s,F} \propto (l_M / l_F)^{1/2}$
Heat flux (kW/m^2)[b]	$\dot{q}''_M / \dot{q}''_F = (l_M / l_F)^{1/2}$
Water droplet size (mm)	$d_M / d_F = (l_M / l_F)^{1/2}$
Water density (mm/min)	$\dot{q}''_{w,M} / \dot{q}''_{w,F} = (l_M / l_F)^{1/2}$
Water flow rate (l/min)	$\dot{q}_{w,M} / \dot{q}_{w,F} = (l_M / l_F)^{5/2}$
Operating pressure (bar)	$P_M / P_F = l_M / l_F$
Response time index, RTI	$\mathrm{RTI}_M / \mathrm{RTI}_F = (l_M / l_F)^{3/4}$

M is model scale and *F* is full scale

[a] Assume $\Delta H_{c,F} = \Delta H_{c,M}$

[b] The scaling of the conductive and radiative heat flux could deviate from the scaling law. The scaling of conductive heat flux depends on the conductive and radiative heat flux. Details can be found in Sect. 18.5

ten percent of the wall thickness below the interior wall surface. Clearly, it shows that there is very good correlation between the full scale and the medium scale. Although the internal wall temperatures in the small scale is slightly lower at some positions, very good correlation can also be found between the full scale and the small scale. Most data lie close to the equal line.

18.9 Summary

Scaling has been successfully applied throughout the development of fire safety science in the past several decades. It is a very powerful and cost-effective tool to obtain valuable information on fire development and suppression, fire characteristics, smoke movement and smoke control, etc.

Scaling theory that has been developed is depicted in this chapter in detail for understanding its mechanism in support of further development of more advanced scaling methods. The focus is on the Froude scaling method which is the most common one used in fire safety science. Scaling of convective heat transfer, radiative heat transfer, and heat conduction is investigated as well as scaling of water sprays, response time of sprinklers, and combustible materials. A list of scaling correlations is given in Table 18.1.

Heat conduction can be scaled very well. Convective heat transfer can be scaled very well for turbulent flows in model tunnels with the same relative roughness. The convective heat transfer for laminar flows in model scales may be slightly overestimated.

Radiative heat flux may be a time-dependent variable during a fire, and emission and absorption of radiation by the walls in model scales are generally overestimated. However, radiation is scaled reasonably well by the fire itself. This could result in a slight difference in gas temperatures between scales.

It should always be kept in mind that the scaling techniques presented here can only produce scenarios similar to full scales in model scales, rather than accurate results. Despite this, the tested fires themselves are still realistic fires.

References

1. Heskestad G (1975) Physical Modeling of Fire. Journal of Fire & Flammability 6:253–273
2. Quintiere JG (1989) Scaling Applications in Fire Research. Fire Safety Journal 15:3–29
3. Ingason H In-Rack Fire Plumes. In: Fire Safety Science – Proceedings of the Fifth International Symposium, Melbourne, Australia, 3–7 March 1997. IAFSS, pp 333–344
4. Perricone J, Wang M, Quintiere J (2007) Scale Modeling of the Transient Thermal Response of Insulated Structural Frames Exposed to Fire. Fire Technology 44 (2):113–136
5. Croce PA, Xin Y (2005) Scale modeling of quasi-steady wood crib fires in enclosures. Fire Safety Journal Vol. 40:245–266

6. Li YZ, Hertzberg T (2013) Scaling of internal wall temperatures in enclosure fires. SP Report 2013:12. SP Technical Research Institute of Sweden, Borås, Sweden
7. Heskestad G (2002) Scaling the interaction of water sprays and flames. Fire Safety Journal 37:535–548
8. Heskestad G (2003) Extinction of gas and liquid pool fires with water spray. Fire Safety Journal 38:301–317
9. Quintiere J.G., Su G.Y., N. S (2007) Physical scaling for water mist fire suppression – a design application. International Journal on Engineering Performance-Based Fire Codes 9 (2):87–108
10. Yu H.Z., Zhou X.Y., Ditch B.D. Experimental validation of Froude-modeling-based physical scaling of water mist cooling of enclosure fires. In: 9th International Symposium on Fire Safety Science (Poster), Karlsruhe, Germany, 21–26 September 2008. IAFSS, pp 553–564
11. Jayaweera T.M., Yu H.Z. (2008) Scaling of fire cooling by water mist under low drop Reynolds number conditions. Fire Safety Journal 43:63–70
12. Yu H.Z. Physical scaling of water mist suppression of pool fires in enclosures. In, College Park, MD, 2011. 10th International Symposium on Fire Safety Science.
13. Bettis RJ, Jagger SF, Wu Y (1993) Interim Validation of Tunnel Fire Consequence Models: Summary of Phase 2 Tests. Health and Safety Executive, Buxton, Derbyshire, UK
14. Oka Y, Atkinson GT (1995) Control of Smoke Flow in Tunnel Fires. Fire Safety Journal 25:305–322
15. Wu Y, Bakar MZA (2000) Control of smoke flow in tunnel fires using longitudinal ventilation systems – a study of the critical velocity. Fire Safety Journal 35:363–390
16. Ingason H, Li YZ (2010) Model scale tunnel fire tests with longitudinal ventilation. Fire Safety Journal 45:371–384
17. Ingason H, Li YZ (2011) Model scale tunnel fire tests with point extraction ventilation. Journal of Fire Protection Engineering 21 (1):5–36
18. Ingason H (2007) Model Scale Railcar Fire Tests. Fire Safety Journal 42 (4):271–282
19. Vauquelin O, Telle D (2005) Definition and experimental evaluation of the smoke "confinement velocity" in tunnel fires. Fire Safety Journal 40:320–330
20. Li YZ, Lei B, Ingason H (2010) Study of critical velocity and backlayering length in longitudinally ventilated tunnel fires. Fire Safety Journal 45:361–370
21. Li YZ, Lei B, Ingason H (2011) The maximum temperature of buoyancy-driven smoke flow beneath the ceiling in tunnel fires. Fire Safety Journal 46 (4):204–210
22. Li YZ, Ingason H (2012) The maximum ceiling gas temperature in a large tunnel fire. Fire Safety Journal 48:38–48
23. Li YZ, Lei B, Ingason H (2013) Theoretical and Experimental Study of Critical Velocity for Smoke Control in a Tunnel Cross-Passage. Fire Technology 49 (2):435–449
24. Li YZ, Lei B, Ingason H (2012) Scale modeling and numerical simulation of smoke control for rescue stations in long railway tunnels. Journal of Fire Protection Engineering 22 (2):101–131
25. Lönnermark A, Lindström J, Li YZ (2011) Model-scale metro car fire tests. SP Report 2011:33. SP Technical research Institute of Sweden, Borås, Sweden
26. Lönnermark A, Lindström J, Li YZ, Claesson A, Kumm M, Ingason H (2012) Full-scale fire tests with a commuter train in a tunnel. SP Report 2012:05. SP Technical Research Institute of Sweden, Borås, Sweden
27. Ingason H (2008) Model scale tunnel tests with water spray. Fire Safety Journal 43 (7):512–528
28. Li YZ, Ingason H (2013) Model scale tunnel fire tests with automatic sprinkler. Fire Safety Journal 61:298–313
29. Li YZ, Ingason H (2011) Model scale tunnel fire tests - Automatic sprinklers SP Report 2011:31 SP Technical Research Institute of Sweden, Borås, Sweden
30. Quintiere JG Fire behaviour in building compartments. In: Proceedings of the Combustion Institutes, 2002. pp 181–193

31. Cheremisinoff N (1986) Encyclopedia of Fluid Mechanics, Volume 3: Gas-Liquid Flows. Gulf Publishing Company, Houston, Texas
32. Schlichting H (1968) Boundary-layer theory. 6th edn. McGraw-Hill, New York.
33. Dembele S, Wen JX, Sacadura JF (2000) Analysis of the two-flux model for predicting water spray transmittance in fire protection applications. Journal of Heat Transfer 122 (1):183–186
34. Dombrowski N., Wolfsohn DL. (1972) The atomization of water by swirl spray pressure nozzles. Trans Inst Chem Engrs 50:259–269
35. Tewarson A (2002) Generation of Heat and Chemical Compounds in Fires. In: DiNenno PJ, Drysdale D, Beyler CL et al. (eds) The SFPE Handbook of Fire Protection Engineering. Third edition edn. National Fire Protection Association, Quincy, MA, USA, pp 3–82 – 83–161
36. Heskestad G (1988) Quantification of thermal responsiveness of automatic sprinklers including conduction effects. Fire Safety Journal 14:113–125
37. Ruffino P., Di Marzo M. (2003) Temperature and Volumetric Fraction Measurements in a Hot Gas Laden with Water Droplets. Journal of Heat Transfer 125 (2):356–364
38. Ruffino P., Di Marzo M. (2002) The Effect of Evaporative Cooling on the Activation Time of Fire Sprinklers. Proceedings of the Seventh International Symposium on Fire Safety Science, pp. 481–492
39. Gavelli F., Ruffino P., Anderson G., Di Marzo M. (1999) Effect of Minute Water Droplets on a Simulated Sprinkler Link Thermal Response. NIST GCR 99-776. National Institute of Standards and Technology, Maryland
40. Li YZ, Ingason H, Lönnermark A (2014) Fire development in different scales of train carriages. In: 11th International Symposium on Fire Safety Science (IAFSS) New Zealand
41. Li YZ, Ingason H, Lönnermark A (2013) Correlations in different scales of metro carriage fire tests. SP Report 2013:13. SP Technical Research Institute of Sweden, Borås, Sweden